



Research Article

# Controllable thermal conversion of thiomolybdate to active few-layer MoS<sub>2</sub> on alumina for efficient hydrodesulfurization

Mari Vinoba<sup>1</sup>  · R. Navvamani<sup>1</sup> · Hanadi Al-Sheeha<sup>1</sup>

© Springer Nature Switzerland AG 2019

## Abstract

Sulfur removal is the most challenging task in petroleum refineries for upgrading clean fuel from crude oil. In this regard, an efficient Ni–MoS<sub>2</sub> catalyst was prepared using ammonium tetrathiomolybdate (ATM), (NH<sub>4</sub>)<sub>2</sub>MoS<sub>4</sub> as a precursor for hydrodesulfurization (HDS) reaction. ATM was derived by sulfiding an aqueous ammoniacal ammonium heptamolybdate and impregnated on alumina support with and without nickel promoter to form a series of MoS<sub>2</sub>/Al<sub>2</sub>O<sub>3</sub>, and Ni–MoS<sub>2</sub>/Al<sub>2</sub>O<sub>3</sub> catalysts with controlled calcination temperature. The prepared ATM and catalysts were characterized by X-ray diffraction (XRD), Infrared spectroscopy and nitrogen adsorption–desorption. The phase transformation of ATM to MoS<sub>2</sub> was observed by TGA, and number of MoS<sub>2</sub> layer formation was calculated from the frequency difference between the redshift and blueshift by Raman spectrum. The catalytic properties of MoS<sub>2</sub>/Al<sub>2</sub>O<sub>3</sub>, and Ni–MoS<sub>2</sub>/Al<sub>2</sub>O<sub>3</sub> were investigated using thiophene as the model compound for HDS reaction. The HDS rate, C<sub>4</sub> hydrocarbon product distribution and selectivity were quantified by microreactor with refinery gas analyzer system. The prepared MoS<sub>2</sub> catalysts (MoS and NiMoS) at 350 °C showed a better conversion rate than another catalyst due to the synergy between the promoter and few-layered MoS<sub>2</sub> on support. Thus, ATM is a suitable candidate for the formulation of Ni–MoS<sub>2</sub> catalyst at 350 °C for improving thiophene HDS activity.

**Keywords** Molybdenum disulfide · Ammonium tetrathiomolybdate · Hydrodesulfurization · Thiophene

## 1 Introduction

Recent literature reveals that one-third to one-half of the total global energy demand has been fulfilled by fossil fuels [1, 2]. Perhaps the other striking sources across the world, fuels are derived from petroleum refinings such as gasoline, diesel, fuel oil and aviation fuel. Petroleum feedstocks are expected to emit a significant amount of sulfur as SO<sub>x</sub> during combustion that has a direct negative impact on the environment. Thus, environmental objectives have been imposed to implement stringent regulations to control the sulfur level in fuels. Based on the aforementioned, many countries have started focusing

on reducing the sulfur content of diesel fuel to an ultra-low level of about 10 ppm [3]. However, the refineries are facing a significant challenge in achieving the required sulfur specification [4], because the sulfur level in the petroleum fraction varies, and depends on the source of crude oils [5]. The hydrodesulfurization (HDS) is part of the hydro-treating process for removing organosulfur compounds from heavy crude oils using the metal disulfide catalyst. Generally, molybdenum and tungsten are used as active metals along with the promoter nickel/cobalt, which may be obtained by two approaches, which are supported [6, 7] and unsupported catalyst [8, 9]. Notably, the supported catalysts were widely used for HDS process, and prepared

**Electronic supplementary material** The online version of this article (<https://doi.org/10.1007/s42452-019-0361-3>) contains supplementary material, which is available to authorized users.

✉ Mari Vinoba, [vinoba76@gmail.com](mailto:vinoba76@gmail.com); [vmari@kisir.edu.kw](mailto:vmari@kisir.edu.kw) | <sup>1</sup>Petroleum Research Center, Kuwait Institute for Scientific Research, P.O. Box 24885, 13109 Safat, Kuwait.



SN Applied Sciences (2019) 1:340 | <https://doi.org/10.1007/s42452-019-0361-3>

Received: 17 February 2019 / Accepted: 11 March 2019 / Published online: 14 March 2019

SN Applied Sciences  
A SPRINGER NATURE journal

with different methodologies such as sulfiding metal oxide [3, 6], thermal decomposition of thiomolybdate [10, 11], hydrothermal and solvothermal processes [12].

The conventional method reveals that the sulfidation of molybdenum oxides under hydrogen sulfide flow at high-temperature is the critical step, because it gives a mixture of partially converted  $\text{MoS}_2$  and unconverted  $\text{MoO}_x$  [13], and it may decrease HDS activity due to the strong interaction between metal and support [14]. However, the support plays a crucial role in the dispersion of active metals for enhancing the dispersion of surface metals [15]. Hence, a new formulation approach is required to produce an even dispersion of active metal on the support for the production of sulfur-free clean fuel from crude oil. In this regard, the direct sulfided catalyst has been prepared using the thermal decomposition of thiomolybdates and recognized as a simple route than the conventional sulfidation of molybdenum oxides. Thiomolybdates possess tetrahedrally coordinated sulfur atom with molybdenum atom that undergoes a topotactic reaction during the decomposition, as resultant, the sulfide structure is retained in the same precursor [16] that enhances HDS activity.

The unsupported trimetallic HDS catalyst is prepared using different thiometallates precursor with better catalytic activity [17–20]. However, the unsupported catalysts tend to have increased pressure drop, reduced lifespan, and less economic feasibility, whereas, the supported catalyst can be recycled and possesses a long life due to the synergistic properties of active metal and support [21]. The porous support materials are considered as an efficient candidate for uniform dispersion of active constituents over high surface area and suitable pore size for the mobility of reactants inside. Currently, there are a number of supports reported for dispersion of an active metal, such as alumina, silica, carbon, titanium oxide and carbon [22]. Especially, alumina has some advantages like high surface area, good strength, tailoring pore structure, and low cost [23], and more acid sites are available that offers the strong interaction between metal and support, which promotes the hydrotreating and hydrogenation reactions [24, 25]. Hence, the highly dispersed active  $\text{MoS}_2$  or  $\text{WS}_2$  supported catalyst was prepared from thiometallates by thermal decomposition for better catalytic activity and which provides excess sulfur for the simultaneous sulfidation of the promoter without  $\text{H}_2\text{S}$  sulfidation process [26, 27].

In this work, a well-dispersed  $\text{MoS}_2$  on alumina support was synthesized using ammonium tetrathiomolybdate (ATM) as a precursor for  $\text{MoS}_2$ , and Ni as a promoter by incipient wetness impregnation method. The metal sulfide formation was studied as a function of calcination temperature under an inert medium in order to diffuse excess 'S' to convert the promoter as in sulfide form. The

physicochemical properties of synthesized ATM and series of the catalyst with and without promoter (mole ratio 0.3 (Ni/(Ni + Mo))) were characterized using several analytical techniques. The hydrodesulfurization activity of the catalyst was investigated using thiophene as a model compound at atmospheric pressure, and calculated reaction rate and selectivity of  $\text{C}_4$  hydrocarbons. Further, the effect of calcination temperature was also studied, which plays a significant role in the catalytic activity. The synthesized  $\text{MoS}_2/\text{Al}_2\text{O}_3$  and Ni– $\text{MoS}_2/\text{Al}_2\text{O}_3$  catalysts reveal a higher thiophene HDS conversion rate and selectivity, and hence can contribute as efficient catalysts for HDS reactions.

## 2 Experimental section

### 2.1 Synthesis of ammonium tetrathiomolybdate

Ammonium tetrathiomolybdate (ATM) was prepared by sulfidation of ammonical molybdate salt as reported elsewhere [17]. Typically, ammonium heptamolybdate (8.09 mmol,  $(\text{NH}_4)_6\text{Mo}_7\text{O}_{24}\cdot 4\text{H}_2\text{O}$ ) dissolved in the mixture of ammonium hydroxide (60 ml) and water (5 ml). The reaction mixture was purged with hydrogen sulfide ( $\text{H}_2\text{S}$ ) for sulfidation at 25 °C for 60 min, and the temperature was slowly raised to 60 °C with continuous  $\text{H}_2\text{S}$  purging until turn a dark red color. The reaction mixture was kept in an ice bath for crystallization of red ATM crystals, and followed by vacuum filtration, washed several times with cold isopropyl alcohol and dried under vacuum. The prepared ATM was stored under an inert atmosphere and subjected to further characterization and used as a precursor for catalysts preparation.

### 2.2 Preparation of MoS and NiMoS catalysts

The commercial alumina ( $\gamma\text{-Al}_2\text{O}_3$ ) extrudates (Sasol, Germany) was used as a support and synthesized ATM as a precursor for  $\text{MoS}_2$ . The stoichiometric molar ratio of Ni/(Ni + Mo) = 0.3 of ATM precursor and promoter nickel as nitrate salt were dispersed on  $\gamma\text{-Al}_2\text{O}_3$  by incipient wetness impregnation method. The promoter nickel was dispersed on  $\gamma\text{-Al}_2\text{O}_3$  by wet impregnation using nickel, dried at 120 °C. Similarly, ATM/ $\text{Al}_2\text{O}_3$  was prepared without a promoter to evaluate the role of the promoter. The prepared nickel promoted ATM/ $\text{Al}_2\text{O}_3$  was calcined at 300 °C, 350 °C, 400 °C and 450 °C under inert medium and corresponding catalyst were denoted as NiMoS-1, NiMoS-2, NiMoS-3, and NiMoS-4, respectively. Likewise, the other catalyst also prepared from ATM/ $\text{Al}_2\text{O}_3$  by calcined as above temperatures and labeled as MoS-1, MoS-2, MoS-3, and MoS-4, respectively. The prepared

series of MoS and NiMoS catalysts were characterized and evaluated for their catalytic activity.

### 2.3 Characterization of ATM and catalysts

The textural properties of prepared catalysts were analyzed by N<sub>2</sub> adsorption–desorption at 77 K on Micromeritics ASAP 2020. The crystal structure of ATM and catalyst were collected using powder X-ray diffraction (XRD) patterns with Cu-K<sub>α</sub> radiation (λ = 0.1542 nm) on PANalytical PW3040, and unit cells quantified with X'pert PRO software. ATM symmetric and asymmetric vibration modes were recorded with potassium bromide pellet method by Fourier-transform infrared spectroscopy (FTIR), Vertex 70 spectrometer, Bruker. The Raman spectroscopy was recorded for active modes of MoS<sub>4</sub><sup>2-</sup> and MoS<sub>2</sub> structure by Senterra, Bruker. The thermal decomposition pathway of ATM → MoS<sub>3</sub> → MoS<sub>2</sub> and prepared catalysts were performed under N<sub>2</sub> medium at a ramping rate of 10 °C/min from 40 to 800 °C by thermogravimetric analyzer (TGA), Mettler. H<sub>2</sub>-temperature-programmed reduction (TPR) profile of the MoS and NiMoS catalyst were carried out by AMI-300S, Altamira Inc, USA. About 100 mg of each catalyst was placed in a quartz cell, pretreated at 150 °C for 2 h under Ar medium, and cooled to room temperature. TPR was performed using 10% H<sub>2</sub>/Ar flow (30 ml/min), and the sample was increased up to 1000 °C at a ramp rate of 10 °C/min [28]. Thermal conductivity detector (TCD) was used to measure the hydrogen consumption during TPR run.

### 2.4 Evaluation of catalysts for HDS activity

The prepared MoS and NiMoS catalysts were evaluated for HDS activity using thiophene, as reported elsewhere [29]. Typically, about 100 mg of each catalyst was placed in the glass microreactor under continuous purging of hydrogen gas (50 ml/min) into thiophene. The flow of thiophene (feed) was kept at constant by controlling saturator temperature at 5 °C, and thiophene containing hydrogen gas was injected into the reactor at 350 °C over 4.5 h for achieving steady state average values. The reactor outlet was connected to online gas chromatography (Agilent, USA) equipped with a capillary column for flame ionization detector and packed column for thermal conductivity detector for quantification hydrocarbons and gaseous products, respectively. Gas chromatography (GC) analyzed data were collected at a constant interval to calculate the reaction rate and C<sub>4</sub> product selectivity.

The overall HDS conversion rate and selective C<sub>4</sub> hydrocarbon formation rates were calculated according to the following equations:

$$\text{Conversion fraction } (\alpha) = \frac{\eta_i - \eta_o}{\eta_i} \quad (1)$$

$$\text{HDS rate } (\kappa) = \frac{F_i \times \alpha}{m} \quad (2)$$

$$C_4 \text{ hydrocarbon rate} = \chi_i \times \kappa \quad (3)$$

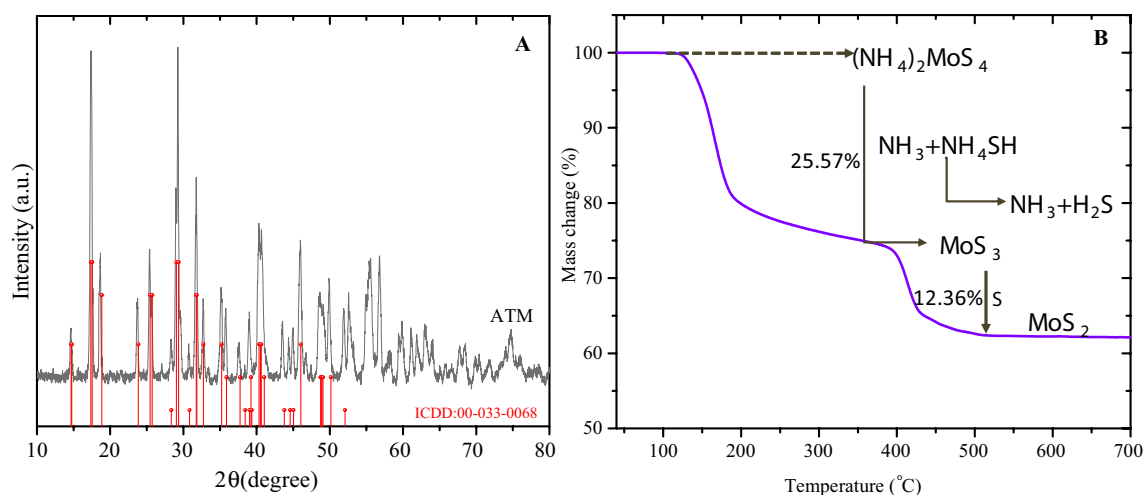
where  $\eta_i$  and  $\eta_o$  are the thiophene concentration (moles) in feed and output of the reactor, respectively, and  $\kappa$ ,  $F_i$  and  $m$  are overall conversion rate (mol h<sup>-1</sup>g<sup>-1</sup>), reactant feed (mol h<sup>-1</sup>) and weight of catalyst (g), respectively. The selectivity of individual C<sub>4</sub> hydrocarbon conversion rate was calculated according to Eq. 3, where  $\chi_i$  is mole fraction of respective C<sub>4</sub> hydrocarbon.

## 3 Results and discussion

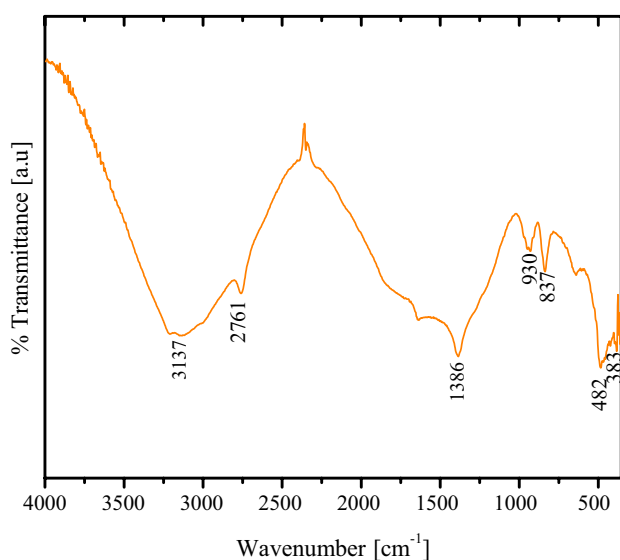
### 3.1 Characterization of ammonium tetrathiomolybdate

Figure 1a shows the X-ray diffraction pattern of ATM precursor that exhibits sharp and narrow peaks with a well-defined orthorhombic crystallographic structure, which complies with a standard ICDD pattern of ATM (00-033-0068). The crystal axis of the synthesized ATM was a = 12.189 Å, b = 9.495 Å, c = 6.94 Å; α = β = γ = 90°, and unit cell volume 804 (Å<sup>3</sup>). The Bragg reflection peaks at 2θ = 17.43°, 18.65°, 25.40°, 28.96°, 29.26°, 31.76°, and 45.96°, corresponds to the crystal faces (hkl) (111), (200), (020), (301), (022), (311), and (413), respectively. Also, Fig. 1b displayed the TGA curve of ATM that shows the plausible conversion pathway of ATM to MoS<sub>2</sub> [30]. The weight loss about 25.72 wt% was observed in the temperature range of 150–330 °C, which attributes to the initial conversion of ATM to MoS<sub>3</sub>, NH<sub>3</sub> and white substance ammonium hydrogen sulfide (NH<sub>4</sub>HS). Subsequently, NH<sub>4</sub>HS decomposed to NH<sub>3</sub> and H<sub>2</sub>S. Furthermore, 12.36 wt% loss occurred in the temperature range 380–500 °C due to the decomposition of the intermediate MoS<sub>3</sub> to MoS<sub>2</sub>. The overall weight loss in the conversion of ATM to MoS<sub>2</sub> was 38.08 wt%, which complies with theoretical stoichiometric weight loss (38.46 wt%). Thus, TGA confirms the formation of MoS<sub>2</sub> by thermal decomposition of ATM through intermediate MoS<sub>3</sub> and elimination of two-mole ammonia and one-mole hydrogen sulfide.

Figure 2 shows the FT-IR spectrum of ATM displays their particular vibration band of Mo-S at 383 and 482 cm<sup>-1</sup> corresponding to strong and stretching modes, respectively [31]. The other band observed at 3137 cm<sup>-1</sup>, and 1386 cm<sup>-1</sup> were attributed to stretching and bending vibration of N-H bands, respectively, and the weak hydrogen bond at 2761 cm<sup>-1</sup>. Also, there are some minor peaks observed which might be an association of Mo = O groups



**Fig. 1** XRD diffraction pattern (a) and TG curve (b) for the prepared ammonium tetrathiomolybdate



**Fig. 2** FTIR spectrum of ammonium tetrathiomolybdate  $(\text{NH}_4)_2\text{MoS}_4$

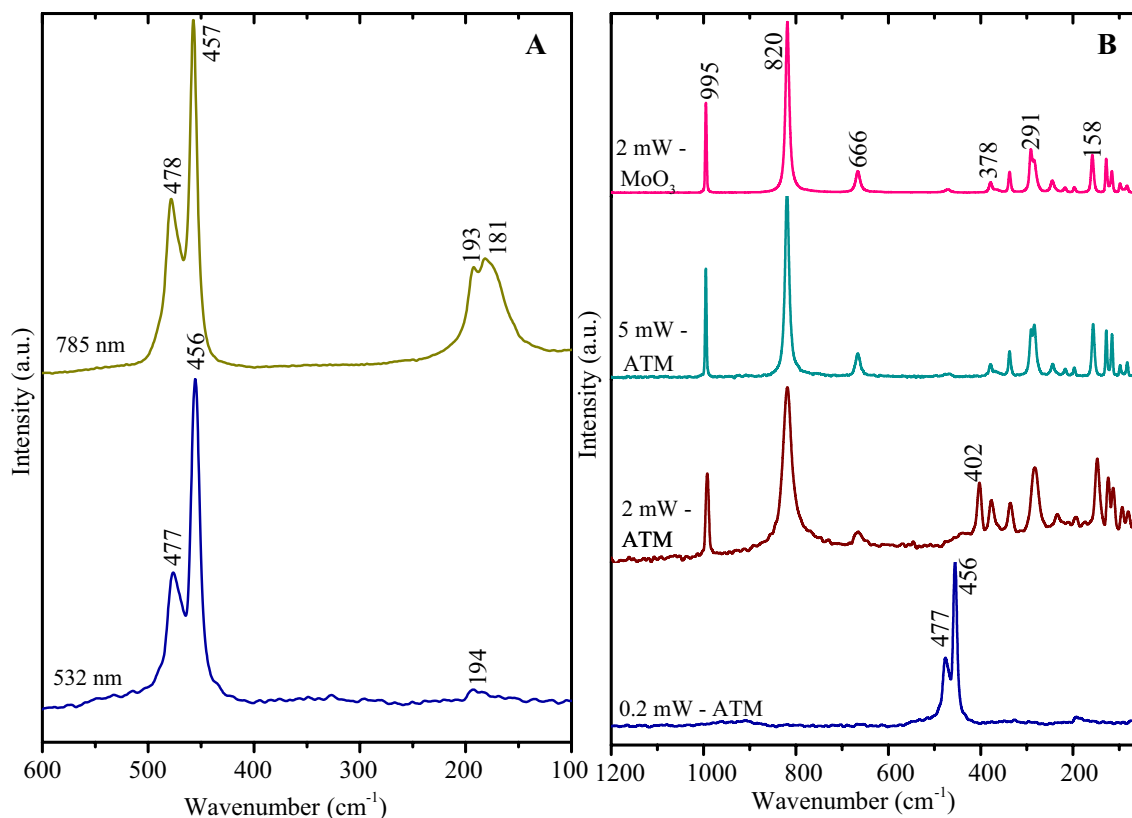
between the sulfide surface and environment. Figure 3 shows Raman spectra of ATM at two different wavelengths, visible (532 nm) and near infra-red (785 nm) regions. The tetrahedral  $[\text{MoS}_4]^{2-}$  possesses four active Raman characteristic modes as  $\nu_1$  ( $A_1$ ),  $\nu_2$  ( $E$ ),  $\nu_3$  ( $F_2$ ), and  $\nu_4$  ( $F_2$ ), in which the asymmetric stretching ( $\nu_3$ ) and symmetric ( $\nu_1$ ) vibration of a  $\text{Mo}=\text{S}$  bond in ATM, were observed at 477 and 456  $\text{cm}^{-1}$  in the both 532 and 785 nm regions (Fig. 3a). The other two Raman active modes of  $\delta(\text{MoS}_4)$  [ $\nu_2(E) + \nu_4(F_2)$ ] in 785 nm exhibits strong band at 193  $\text{cm}^{-1}$  and a medium band at 181  $\text{cm}^{-1}$ , whereas the visible region appears as strong band at 194  $\text{cm}^{-1}$  in 532 nm [31, 32].

In addition, the stability of ATM was also evaluated with different laser power at 532 nm (Fig. 3B), as  $\text{MoS}_4^{2-}$  ion is unstable at high laser power. Photochemical decomposition of ATM is minimized at a low power of 0.2 mW and shows all Raman active modes. However, ATM decomposes to gas products as ammonia and hydrogen sulfide, and partial conversion of  $\text{MoS}_2$  to  $\text{MoO}_3$  under atmospheric air environment at 2.0 mW laser power. The formation of  $\text{MoS}_2$  was confirmed by the characteristics vibration bands of  $A_{1g}$  (402  $\text{cm}^{-1}$ ),  $E_{2g}$  (387  $\text{cm}^{-1}$ ) and  $E_{1g}$  (378  $\text{cm}^{-1}$ ). Further, it was also verified by surface oxidization of  $\text{MoS}_2$  to stable  $\text{MoO}_3$  with higher laser power (5 mW) under atmospheric condition. The peaks observed at 158, 291, 666, 820, and 990  $\text{cm}^{-1}$  due to symmetric and asymmetric stretch of the terminal oxygen atom of  $\text{Mo}-\text{O}$  complies with the pure  $\text{MoO}_3$  spectrum (2 mW- $\text{MoO}_3$ , Fig. 3b) [33]. Therefore, the Raman spectrum reveals minimum laser power is a suitable condition for ATM without oxidation at atmospheric environment (for example, 0.2 mW at 532  $\text{cm}^{-1}$ ).

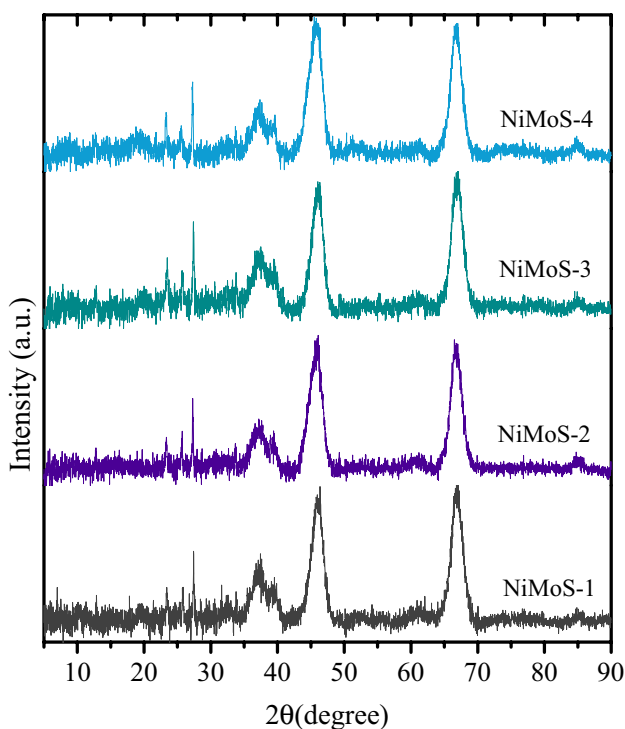
### 3.2 Characterization of MoS and NiMoS catalysts

Figure 4 and S1 show the series of X-ray diffraction patterns of MoS and NiMoS, respectively, and derived by thermal decomposition of ATM/ $\text{Al}_2\text{O}_3$  and nickel supported ATM/ $\text{Al}_2\text{O}_3$  from 300 to 450  $^\circ\text{C}$ . The XRD pattern reveals the poor crystalline structures of 2H- $\text{MoS}_2$  in MoS and NiMoS catalysts. When increasing the decomposition temperature,  $\text{MoS}_4^{2-}$  is slowly converted to  $\text{MoS}_2$  and its corresponding characteristic peak emerges at 200 ( $hkl$ ) as two broad peaks at  $2\theta = 24\text{--}27^\circ$  and  $42\text{--}47^\circ$ . These XRD patterns reveals that the low crystalline  $\text{MoS}_2$  lattice planes were associated with alumina. The characteristic of  $\text{MoS}_2$  peak on MoS and NiMoS catalysts are agreed with ICDD





**Fig. 3** Raman spectra of ammonium tetrathiomolybdate; **a** at 532 nm and 785 nm, and **b** at laser power 0.2 mW, 2 mW and 5 mW, and MoO<sub>3</sub> at 2 mW



**Fig. 4** XRD patterns of NiMoS catalysts

card of MoS<sub>2</sub> (03-065-0160). Some Ni<sub>x</sub>S<sub>x</sub> and MoO<sub>3</sub> peaks were also observed at higher temperature due to surface oxidation [34]. The NiMoS catalyst exhibited its oxide peaks at  $2\theta = 23.33^\circ$ ,  $25.75^\circ$ , and  $27.33^\circ$ , which is in line with ICDD card 00-05-0508. It is expected that MoS<sub>3</sub> diffuse its sulfur atom (MoS<sub>3</sub> → MoS<sub>2</sub>) during the calcination to form nickel sulfide.

The surface area of prepared catalysts was determined by the Brunauer–Emmett–Teller (BET) and pore size by Barrett–Joyner–Halenda (BJH) method. Figure 5 summarizes the textural properties of the prepared catalysts, and Figs. S2 and S3 show the nitrogen adsorption/desorption isotherms of MoS and NiMoS catalyst with hysteresis loop and well-defined pore size distribution. The surface area, pore volume and pore size of alumina support are 228 m<sup>2</sup>/g, 0.86 cm<sup>3</sup>/g, and 98 Å, respectively. Figure 5 reveals the surface area loss in both the MoS and NiMoS catalysts compared to the support that may be due to the filling of the narrow pores by the impregnated metals. On the other hand, the calcination temperature of the catalysts also affects the surface area. There is no remarkable difference in surface area of NiMoS catalyst when the temperature increases from 300 to 350 °C. Whereas, a significant change in surface area was observed when

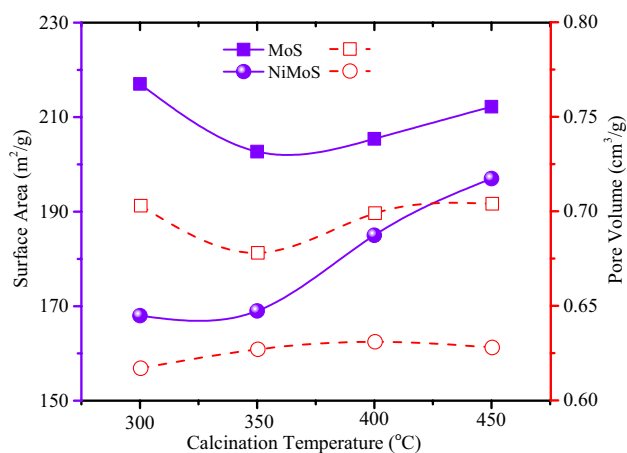


**Fig. 5** The surface area and pore volume of MoS and NiMoS catalysts at calcination temperatures 300 °C, 350 °C, 400 °C and 450 °C

the temperature was increased from 350 to 450 °C (16%). These increase may be due to the evaluation of ammonia, hydrogen sulfide, and elemental sulfur during the decomposition of ATM. Further, about 95–98% of the overall pore size of NiMoS catalysts were retained at different calcination temperature and shows type IV nitrogen adsorption/desorption hysteresis loop (Figs. S2A and S3A). The pore size distribution of MoS and NiMoS catalysts shown in Figs. S2B and S3B.

Fig. S4 and S5 shows the thermal stability of prepared MoS and NiMoS catalysts determined by a thermogravimetric analyzer (TGA). The TG profiles inferred different structural changes of catalysts through a mass change in the range of 40 °C to 800 °C. MoS and NiMoS supported catalysts show about 5–8% weight loss below 180 °C due to the loss of physisorbed moisture from the atmosphere. Also, the TGA curve exhibits a descending order in the weight loss of catalysts with increasing calcination temperature from 300 to 450 °C, due to decomposition of bounded ammonium hydrogen sulfide. MoS-1 and MoS-2 show higher weight loss about 7% than MoS-3 and MoS-4 in this region of 180–480 °C, which is mainly due to the undecomposed intermediate or incomplete MoS<sub>3</sub> phases (Fig. S4). NiMoS catalyst shows the minimum mass loss (~3%) in the same temperature range, which attributes to the low retaining capacity of humidity (Fig. S5). Above 500 °C, the weight loss observed in NiMoS catalyst may be due to the oxidation of Ni<sub>x</sub>S<sub>x</sub> to nickel oxide on support.

Raman spectra confirm the formation of MoS<sub>2</sub> from ATM at different calcination temperatures. The Raman analysis is an indicative technique to identify the formation of hexagonal MoS<sub>2</sub> geometry, which consists of D<sub>6h</sub> (P6<sub>3</sub>/mmc) space group symmetry on the support surface [35]. The structural characteristics of supported MoS<sub>2</sub> and Ni–MoS<sub>2</sub> catalyst indicated a significant amount of

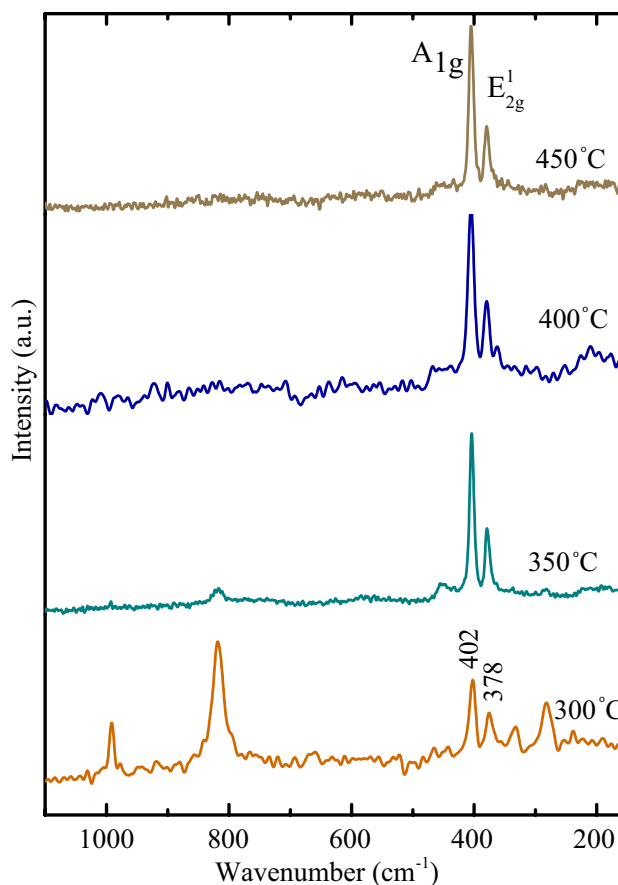


**Fig. 6** Raman spectra of prepared NiMoS catalyst at different calcination temperatures 300, 350, 400 and 450 °C

molybdenum–oxygen stretching at 300 °C. The peak intensity of Mo–O was decreased on calcination at 350 °C and disappeared on calcination temperatures at 400 °C and 450 °C calcined catalyst. On the other hand, the presence of strong bands at 402 and 378 cm<sup>-1</sup> belong to MoS<sub>2</sub>.

Raman spectra of bulk MoS<sub>2</sub> exhibits four active vibration modes such as A<sub>1g</sub>, E<sub>1g</sub>, E<sub>2g</sub><sup>1</sup> and E<sub>2g</sub><sup>2</sup>, that corresponds to out-of-plane vibrations of S atoms, in-plane vibrations of S atoms, in-plane vibrations of Mo–S bond, and in-plane of the rigid atomic bond, respectively [36]. The frequency and intensity of Raman peaks depend on out-of-plane vibrations of the sulfur atoms that soften the redshift at ~402 cm<sup>-1</sup> (A<sub>1g</sub>), and strong in-plane vibration of Mo and S atoms, which stiffens the blueshift at ~380 cm<sup>-1</sup> (E<sub>2g</sub><sup>1</sup>) S atoms. MoS catalysts exhibited E<sub>2g</sub><sup>1</sup> vibration modes in the calcination region of 300 °C to 350 °C. In case of NiMoS catalysts, NiMoS-1 shows MoS<sub>2</sub> and MoO<sub>3</sub> peaks at 300 °C and other NiMoS-2 to NiMoS-4 catalysts indicated active A<sub>1g</sub> and E<sub>2g</sub><sup>1</sup> modes of MoS<sub>2</sub> at calcination temperature 350 to 450 °C (Fig. 6). When increasing the calcination temperature, the redshift of A<sub>1g</sub> peak width slightly increased and E<sub>2g</sub><sup>1</sup> peak intensity reduced in NiMoS catalyst reveals

to reduced stacked  $\text{MoS}_2$  layer along with the  $c$  axis, and existence in-plane defect sites, respectively [37, 38]. Thus, the surface geometry of  $\text{MoS}_2$  varies with stacked layers due to the different vibration modes of Mo and S atoms.

The wavelength difference between  $E_{2g}^1$  and  $A_{1g}$  are fingerprint modes that correspond to the number of layer formation of  $\text{MoS}_2$ . Typically, monolayer formation is denoted when the difference between  $E_{2g}^1$  and  $A_{1g}$  is  $18\text{ cm}^{-1}$ , and the few-layer formation for the difference of  $19\text{ cm}^{-1}$  to  $26\text{ cm}^{-1}$  in bulk crystal [39]. The wavelength difference between  $A_{1g}$  and  $E_{2g}^1$  for NiMoS-1, NiMoS-2, NiMoS-3, and NiMoS-4 catalysts were found to be 24.0, 23.3, 23.0 and  $22.8\text{ cm}^{-1}$ , respectively. Thus, Raman spectra revealed that the NiMoS catalyst, prepared at calcination temperatures from 300 to 450 °C under inert medium, possesses few-layer  $\text{MoS}_2$ . Further, layer formation depends on a function of calcination temperature, which gives descending order of  $\text{MoS}_2$  layer with increasing calcination temperature.

The  $\text{H}_2$ -TPR technique suggested that the interaction between surface  $\text{MoS}_2$  phase and  $\text{MoO}_2$  with support forms a network structured like  $\text{MoS}_2\text{-O-MoO}_2$  [40]. MoS catalysts exhibit four reduction peaks, located at 552, 630, 708 and 863 °C, and whereas NiMoS catalyst shows the two reduction peaks located at 507 and 760 °C (Fig. 7). It is reported that the conventional  $\text{Mo/Al}_2\text{O}_3$  and NiMo/ $\text{Al}_2\text{O}_3$  catalyst shows reduction of  $\text{Mo}^{6+}$  to  $\text{Mo}^{4+}$  on a support surface at 600–800 °C for reduction of tetrahedrally coordinated Mo species [41]. However, the prepared NiMoS catalyst reduced two regions at low-temperature region 400–550 °C and 600–800 °C, which reflects the high hydrogen consumption at low-temperature, and results favor the hydrogenation of highly reactive sulfur species positioned on the edge of  $\text{MoS}_2$  [42, 43]. TPR results also

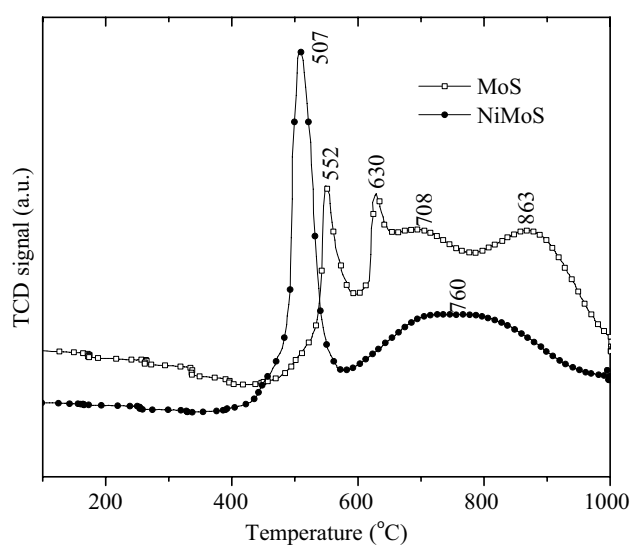


Fig. 7  $\text{H}_2$ -TPR profiles of MoS-3 and NiMoS-3 catalysts

indicated reduction of  $\text{MoS}_3$  ( $\text{Mo}^{6+}$ ) to other Mo oxidation state and its interaction with the support. Moreover, the initial catalyst has Mo and S stoichiometry of  $\text{S/Mo} = 2.3$ , while in the reduced condition, it is expected to be  $\text{S/Mo} = 2.0$ . This might be due to the reduction of sulfur from the hexagonal lattice to the relatively unstable rhombohedral  $\text{MoS}_2$ , which is in agreement with the DFT calculation [44].

### 3.3 Hydrodesulfurization on MoS and NiMoS catalysts

The  $\text{MoS}_2$ -based catalysts with and without promoter on alumina support were prepared at different temperatures, 300, 350, 400 and 450 °C, and tested for thiophene HDS activity at 350 °C (Fig. S6). The various products were obtained by thiophene HDS reaction such as  $\text{C}_4$  (2-butenes, 1-butene, n-butane, i-butane, and butadiene),  $\text{C}_3$  (propane and propene),  $\text{C}_2$  (ethane and ethene) and  $\text{C}_1$  (methane) compounds [45, 46]. The desulfurized products including  $\text{C}_1\text{-C}_3$  and  $\text{C}_4$  hydrocarbons were quantified using online refinery gas analyzer (RGA) system with calibrated Agilent refinery gas mixture P/N 5190-0519. The initial conversion was the same for both MoS and NiMoS catalysts, later significant changes in activity on NiMoS catalyst were observed, which shows higher HDS rate. The higher activity may correspond to the role of promoter as well as higher hydrogenation function of NiMoS catalyst (Fig. S6B). Thus, the thiophene HDS rate depends on the calcination temperature of the catalyst, and the order of HDS activity at equilibrium condition as follows  $350\text{ °C} > 300\text{ °C} > 400\text{ °C} > 450\text{ °C}$ .

The overall NiMoS catalysts represented higher conversion rate than MoS catalysts due to the presence of Ni

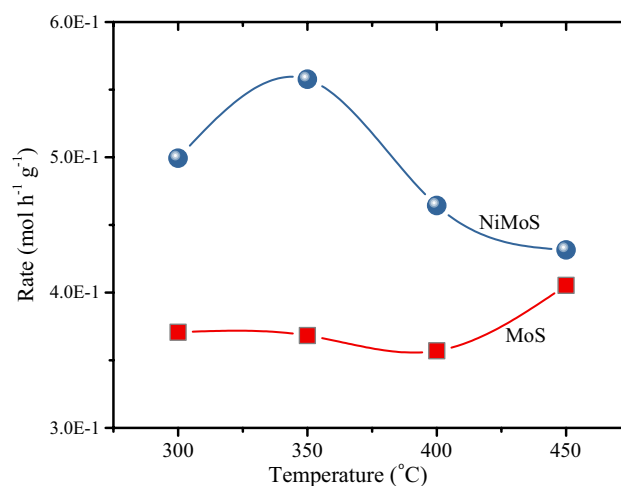
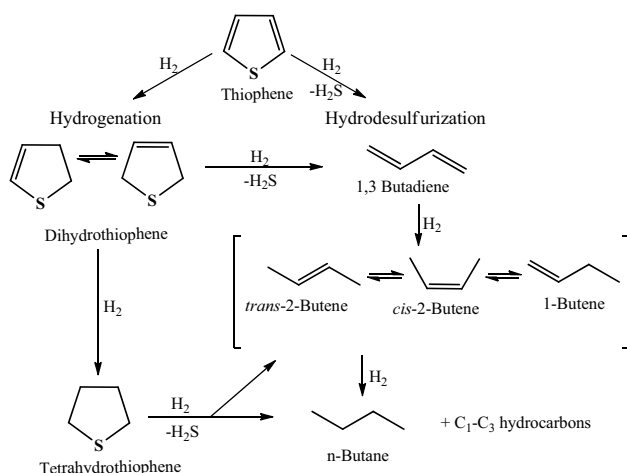


Fig. 8 The effect of calcination temperature of MoS and NiMoS catalysts for thiophene HDS rate

promoter, and has good hydrogenation ability, as shown in Fig. 8. However, the HDS activity also depends on the presence of few layers  $\text{MoS}_2$  and weakly bonded sulfur on the surface of NiMoS catalyst that is affected by calcination temperature. It was observed that the HDS rate enhanced in both catalysts calcined at 350 °C due to the formation of active few-layer  $\text{MoS}_2$  from  $\text{MoS}_3$ . About 34% higher HDS rate was observed at 350 °C calcined NiMoS than MoS because the Ni acts as a promoter. Upon increasing the calcination temperature from 350 to 450 °C, decline trend in activity revealed in both catalyst, which might be the partial formation of inactive  $\text{Mo}_x\text{S}_x$  instead of few-layer  $\text{MoS}_2$  at higher calcination temperature. The pure alumina support has only Lewis acid sites, whereas Mo-dispersed  $\text{Al}_2\text{O}_3$  catalysts have both Lewis and Brønsted acid sites on the surface due to the molybdenum species bounded to the alumina surface through oxygen bridges with surface OH groups. Further, the generation of weak acid protonic sites via dissociative  $\text{H}_2\text{S}$  reactions located at the edges of  $\text{MoS}_2$  creates the anion vacancies that also play a crucial role in the HDS mechanism.

The plausible pathway of thiophene HDS may occur through different intermediates by hydrogenation of C=C bond and the direct desulfurization of the C-S bond (Scheme 1). The hydrogenation process reveals the formation of butenes and butane, through dihydrothiophenes and tetrahydrothiophene intermediates, respectively. The weaker C-S bonds of thiophene are more reactive on the catalyst surface, and they undergo hydrogenolysis of C-S bond through dihydrothiophene to produce butadiene, and subsequently hydrogenated to be produced as butane and butenes, and formation of 1,3 butadiene was not observed on any catalysts [45]. The thiophene HDS reaction mechanism indicated that 1,3 butadiene is a



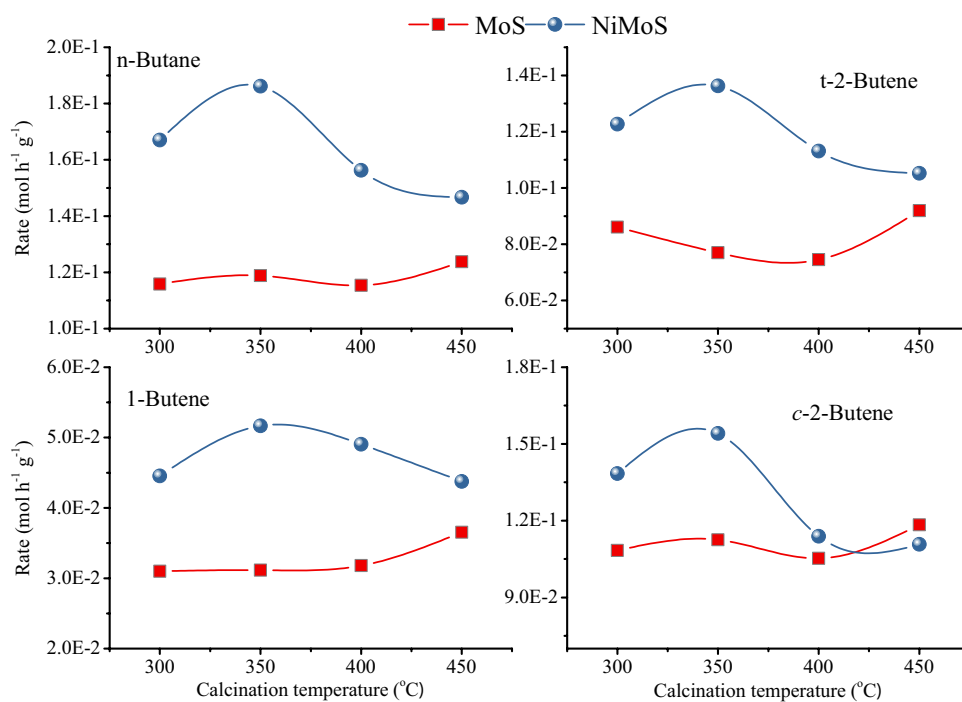
**Scheme 1** Possible thiophene HDS network on the  $\text{MoS}_2$ -based catalyst

primary product, which is expected to decrease with conversion and subsequent hydrogenation to 1-butene (*cis* and *trans* butenes). The butadiene rapidly converted to the secondary products in the presence of  $\text{H}_2$  on catalysts by hydrogenation [47]. The hydrogenated intermediates dihydrothiophene and tetrahydrothiophene were also not detected during reaction because of rapid conversion to butane in the presence of  $\text{H}_2$  environment. However, the hydrogenation of 1,3 butadiene is faster than tetrahydrothiophene [48], which is evidenced by the formation of significant amount of products like  $\text{C}_4$  hydrocarbons of butenes (1-butene, 2-butene, and *n*-butene) and butane, along with the smaller yield of iso-butane, iso-butene and cracked (methane, ethane, and propene) products. Hence, the *n*-butane, 1-butene, *cis*-2-butene, and *trans*-2-butene were quantified, and the product formation rate was calculated as a function of calcination temperature, as shown in Fig. 9.

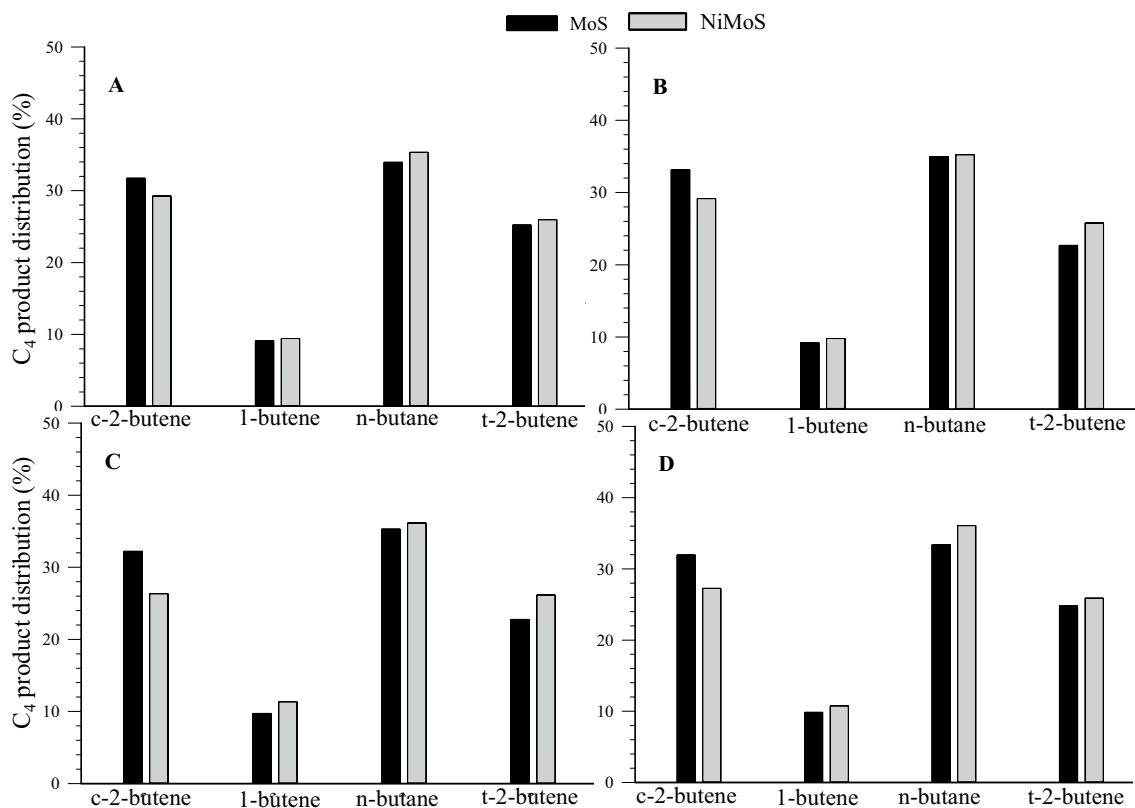
Figure 9 shows each  $\text{C}_4$  hydrocarbon formation rate as a function of calcination temperature from 300 to 450 °C. It is observed that rates of formation of *n*-butane, 1-butene, *cis*-2-butene, and *trans*-2-butene were higher on NiMoS than MoS catalyst calcined at 350 °C catalyst and were about 1.57, 1.66, 1.37 and 1.77-fold, respectively, which might be due to the influence of Ni promoter. The butene formation rate remains constant with increasing calcination temperature and/or presence of Ni promoter. As discussed previously, the number of few-layer  $\text{MoS}_2$  and weakly bonded sulfur on the catalyst surface contributes to the rate of formation of butenes. The number of layer of  $\text{MoS}_2$  from  $\text{MoS}_4^{2-}$  decreases with increasing calcination temperature as supported by Raman spectrum and the same trend is expected for HDS of thiophene. Based on this, the rate of formation of butene has to decrease, but the weakly bonded sulfur on surface catalyst stimulates the isomerization of 1-butene to *cis*- and *trans*-2-butene. Hence, the butenes formation rates were almost similar either in the presence or absence of Ni promoter for the catalysts calcined at 450 °C. Overall, the prepared MoS and NiMoS catalysts reveal that the ratio of formation rate of *cis*- to *trans*-2-butene was higher at 350 °C than other calcination temperatures due to the availability of weakly bonded sulfur on the surface of the catalyst.

Figure 10 shows the distribution of  $\text{C}_4$  hydrocarbon produced on MoS and NiMoS catalysts by thiophene HDS at 350 °C. The layer formation on NiMoS catalysts and the enhanced hydrogen capacity evidenced by Raman and TPR analysis has influenced the product distribution as well. Figure 10 indicates that the selectivity of *cis*-2-butene is slightly less over NiMoS than MoS at all the calcination temperature. The result demonstrated that the presence of promoter Ni does not have a significant impact on the formation of *cis*-2-butene. The MoS catalysts influenced





**Fig. 9** The thiophene HDS product formation rate on different calcined MoS and NiMoS catalysts



**Fig. 10** The C<sub>4</sub> hydrocarbon product distribution on different calcined MoS and NiMoS catalysts; calcination at 300 °C (a), 350 °C (b), 400 °C (c), and 450 °C (d)

the formation of n-butane, 1-butene, and *trans*-2-butene, whereas, NiMoS that does not increase the formation of *cis*-2-butene, which might be due to the reversible reaction between *cis*-2-butene and *trans*-2-butene. Thus, there exists a thermodynamic equilibrium between n-butane and butenes (1-butene and 2-butenes) about 35% and 65%, respectively. The two isomerized products of 1-butenes such as *cis*-2-butene and *trans*-2-butene displayed with the ratio are nearly one. The results also depicted that product selectivity distribution was high for n-butane and less for 1-butene among the other C<sub>4</sub> products.

## 4 Conclusions

The characteristics of synthesized ATM such as orthorhombic phase, the strong and stretching vibration mode of Mo–S bond, the asymmetric stretching and symmetric vibration of a Mo=S bond, and thermal conversion of ATM → MoS<sub>3</sub> → MoS<sub>2</sub> were confirmed by XRD, FT-IR spectra, Raman spectra, and TGA analysis, respectively. A series of few-layer MoS<sub>2</sub> catalysts with and without nickel promoter on alumina was prepared by thermal decomposition of impregnated ATM at different calcination temperatures. The Raman spectra revealed that the number of MoS<sub>2</sub> layer formation decreased on increasing the calcination temperatures. The surface area of MoS and NiMoS catalyst was increased about 4 and 16%, respectively, when the calcination temperature increased from 350 to 450 °C due to the thermal expansion. TPR exhibits the presence of well-defined and highly reactive sulfur species that are weakly bonded and located on the surface of NiMoS and MoS catalysts. Based on the characteristics of NiMoS catalysts, higher HDS conversion rate and selectivity for C<sub>4</sub> hydrocarbons of n-butane and butenes were observed when compared to MoS catalyst at 350 °C, due to the presence of promoter that enhanced the hydrogen capacity on MoS<sub>2</sub>. Rates of formation of n-butane, 1-butene, *cis*-2-butene, and *trans*-2-butene were higher on NiMoS catalyst than MoS catalysts calcined at 350 °C and were about 1.57, 1.66, 1.37 and 1.77-fold, respectively. Finally, synthesis of the MoS<sub>2</sub> catalysts by thiomolybdate precursor was found to be a simple route compared to traditional sulfided route for catalysts preparation. Thus, the NiMoS<sub>2</sub> catalysts synthesized by thiomolybdate precursor also proves to be an efficient catalyst for HDS reaction.

**Acknowledgements** This work was supported through petroleum research center funded by the Kuwait Institute for Scientific Research (KISR).

## Compliance with ethical standards

**Conflict of interest** The authors declare that they have no conflict of interest.

## References

1. Shafiee S, Topal E (2009) When will fossil fuel reserves be diminished? Energy Policy 37:181–189
2. Rana MS, Vinoba M, AlHumaidan FS (2017) Sustainability challenges in oil and gas development in the Middle East and North Africa. Curr Sustain Renew Energy Rep 4:232–244
3. Stanislaus A, Marafi A, Rana MS (2010) Recent advances in the science and technology of ultra low sulfur diesel (ULSD) production. Catal Today 153:1–68
4. Han J, Forman GS, Elgowainy A, Cai H, Wang M, DiVita VB (2015) A comparative assessment of resource efficiency in petroleum refining. Fuel 157:292–298
5. Ancheyta J (2016) Deactivation of heavy oil hydroprocessing catalysts: fundamentals and modeling. Wiley, Hoboken
6. Dhar GM, Srinivas BN, Rana MS, Kumar M, Maity SK (2003) Mixed oxide supported hydrodesulfurization catalysts—a review. Catal Today 86:45–60
7. Kostova NG, Krалева E, Spojakina AA, Godocikova E, Balaz P (2007) Effect of preparation technique on the properties of Mo-containing Al-MCM-41. J Mater Sci 42:3321–3325
8. Chianelli RR, Berhault G, Torres B (2009) Unsupported transition metal sulfide catalysts: 100 years of science and application. Catal Today 147:275–286
9. Albersberger S, Hein J, Schreiber MW, Guerra S, Han JY, Gutierrez OY, Lercher JA (2017) Simultaneous hydrodenitrogenation and hydrodesulfurization on unsupported Ni-Mo-W sulfides. Catal Today 297:344–355
10. Nogueira A, Znaiguia R, Uzio D, Afanasiev P, Berhault G (2012) Curved nanostructures of unsupported and Al<sub>2</sub>O<sub>3</sub>-supported MoS<sub>2</sub> catalysts: synthesis and HDS catalytic properties. Appl Catal A 429:92–105
11. Krishnan U, Kaur M, Singh K, Kumar M, Kumar A (2019) A synoptic review of MoS<sub>2</sub>: synthesis to applications. Superlattice Microst 128:274–297
12. Sollner J, Gonzalez DF, Leal JH, Eubanks TM, Parsons JG (2017) HDS of dibenzothiophene with CoMoS<sub>2</sub> synthesized using elemental sulfur. Inorg Chim Acta 466:212–218
13. Massoth FE (1975) Studies of molybdena-alumina catalysts: IV. Rates and stoichiometry of sulfidation. J Catal 36:164–184
14. Prins R (2001) Catalytic hydrodenitrogenation. Adv Catal 46:399–464
15. Rana MS, Ramirez J, Gutierrez-Alejandre A, Ancheyta J, Cedeno L, Maity SK (2007) Support effects in CoMo hydrodesulfurization catalysts prepared with EDTA as a chelating agent. J Catal 246:100–108
16. Diehl EF, Tamilia J, Pollack S (1991) In: Davis H (ed) Proceedings of the 12th North American Catalysis Society Meeting, pp PD-38 B. Lexington, KY
17. Romero L, Valle MA, Rivera RR, Alonso G, Borja MA, Fuentes S, Delgado FP, Reyes JC (2015) MoS<sub>2</sub> catalysts derived from n-methylenediammonium thiomolybdates during HDS of DBT. Catal Today 250:66–71
18. Acuña RH, Núñez GA, Delgado FP, Romero JL, Berhault G, Muñoz EMR (2015) Unsupported trimetallic CoMoW sulfide HDS catalysts prepared by in situ decomposition of sulfur-containing precursors. Catal Today 250:28–37

19. Yi Y, Jin X, Wang L, Zhang Q, Xiong G, Liang C (2011) Preparation of unsupported Ni-Mo-S catalysts for hydrodesulfurization of dibenzothiophene by thermal decomposition of tetramethylammonium thiomolybdates. *Catal Today* 175:460–466
20. Lumbreras JA, Huirache-Acuña R, Rivera-Muñoz EM, Berhault G, Alonso-Núñez G (2010) Unsupported Ni/Mo(W)S<sub>2</sub> catalysts from hexamethylenediammonium thiomolybdates precursors: in situ activation during the HDS of DBT. *Catal Lett* 134:138–146
21. Gajardo P, Declerck-Grimee RI, Delvaux G, Olodo P, Zabala JM, Canesson P, Grange P, Delmon B (1977) Comparative study of unsupported and supported Co-Mo hydrodesulphurisation catalysts. *J Less Common Met* 54:311–320
22. Topsøe H, Clausen BS, Massoth FE (1996) Hydrotreating catalysis. In: Anderson JR, Boudart M (eds) *Catalysis: science and technology*, Springer, Berlin, pp 1–269
23. Zhang D, Liu WQ, Liu YA, Etim UJ, Liu XM, Yan ZF (2017) Pore confinement effect of MoO<sub>3</sub>/Al<sub>2</sub>O<sub>3</sub> catalyst for deep hydrodesulfurization. *Chem Eng J* 330:706–717
24. Roukoss C, Laurenti D, Devers E, Marchand K, Massin L, Vrinat M (2009) Hydrodesulfurization catalysts: promoters, promoting methods and support effect on catalytic activities. *C R Chim* 12:683–691
25. Farag H, Whitehurst DD, Sakanishi K, Mochida I (1999) Carbon versus alumina as a support for Co-Mo catalysts reactivity towards HDS of dibenzothiophenes and diesel fuel. *Catal Today* 50:9–17
26. Iriarte V, Cruz-Reyes J, Del Valle M, Alonso G, Fuentes S, Paraguay-Delgado F, Romero-Rivera R (2017) Trimetallic NiMoW sulfide catalysts by the thermal decomposition of thiosalt blends for the hydrodesulfurization of dibenzothiophene. *React Kinet Mech Catal* 121:593–605
27. Yi YJ, Jin X, Wang L, Zhang QM, Xiong G, Liang CH (2011) Preparation of unsupported Ni-Mo-S catalysts for hydrodesulfurization of dibenzothiophene by thermal decomposition of tetramethylammonium thiomolybdates. *Catal Today* 175:460–466
28. Lai W, Song W, Pang L, Wu Z, Zheng N, Li J, Zheng J, Yi X, Fang W (2013) The effect of starch addition on combustion synthesis of NiMo–Al<sub>2</sub>O<sub>3</sub> catalysts for hydrodesulfurization. *J Catal* 303:80–91
29. Trejo F, Rana MS, Ancheyta J, Rueda A (2012) Hydrotreating catalysts on different supports and its acid-base properties. *Fuel* 100:163–172
30. Wang HW, Skeldon P, Thompson GE (1998) Thermogravimetric-differential thermal analysis of the solid-state decomposition of ammonium tetrathiomolybdate during heating in argon. *J Mater Sci* 33:3079–3083
31. Müller A, Weinstock N, Schulze H (1972) Laser-Raman-Spektren der Ionen MoS<sub>4</sub><sup>2-</sup>, WS<sub>4</sub><sup>2-</sup>, MoOS<sub>3</sub><sup>2-</sup> und WOS<sub>3</sub><sup>2-</sup> in wässriger Lösung sowie der entsprechenden kristallinen Alkalisalze. *Spectrochim Acta, Part A* 28:1075–1082
32. Aljowder OA (2004) Solid state imposed vibrational coupling between  $\nu(1)$  and  $\nu(3)$  modes of tetrahedral ions. *Spectrochim Acta Part A* 60:2837–2841
33. Windom BC, Sawyer WG, Hahn DW (2011) A Raman spectroscopic study of MoS<sub>2</sub> and MoO<sub>3</sub>: applications to tribological systems. *Tribol Lett* 42:301–310
34. Pedraza F, Fuentes S (2000) Ni-Mo and Ni-W sulfide catalysts prepared by decomposition of binary thiomolybdates. *Catal Lett* 65:107–113
35. Terrones H, Corro ED, Feng S, Poumirol JM, Rhodes D, Smirnov D, Pradhan NR, Lin Z et al (2014) New first order Raman-active modes in few layered transition metal dichalcogenides. *Sci Rep* 4:4215
36. Verble JL, Wieting TJ (1970) Lattice Mode Degeneracy in MoS<sub>2</sub> and other layer compounds. *Phys Rev Lett* 25:362–365
37. Miao J, Xiao FX, Yang HB, Khoo SY, Chen J, Fan Z, Hsu YY, Chen HM et al (2015) Hierarchical Ni-Mo-S nanosheets on carbon fiber cloth: a flexible electrode for efficient hydrogen generation in neutral electrolyte. *Sci Adv* 1:1500259
38. Kong D, Wang H, Cha JJ, Pasta M, Koski KJ, Yao J, Cui Y (2013) Synthesis of MoS<sub>2</sub> and MoSe<sub>2</sub> films with vertically aligned layers. *Nano Lett* 13:1341–1347
39. Lee C, Yan H, Brus LE, Heinz TF, Hone J, Ryu S (2010) Anomalous lattice vibrations of single- and few-layer MoS<sub>2</sub>. *ACS Nano* 4:2695–2700
40. Okamoto Y, Kato A, Usman Rinaldi N, Fujikawa T, Koshika H, Hiro-mitsu I, Kubota T (2009) Effect of sulfidation temperature on the intrinsic activity of Co–MoS<sub>2</sub> and Co–WS<sub>2</sub> hydrodesulfurization catalysts. *J Catal* 265:216–228
41. Brito JL, Laine J (1993) Reducibility of Ni-Mo/Al<sub>2</sub>O<sub>3</sub> catalysts: a TPR study. *J Catal* 139:540–550
42. Li XS, Xin Q, Guo XX, Grange P, Delmon B (1992) Reversible hydrogen adsorption on MoS<sub>2</sub> studied by temperature-programmed desorption and temperature-programmed reduction. *J Catal* 137:385–393
43. Vasudevan PT, Zhang F (1994) Characterization of supported molybdenum sulfide catalyst ex ammonium tetrathiomolybdate. *Appl Catal A* 112:161–173
44. Sun M, Nelson AE, Adjaye J (2005) Adsorption and dissociation of H<sub>2</sub> and H<sub>2</sub>S on MoS<sub>2</sub> and NiMoS catalysts. *Catal Today* 105:36–43
45. Salnikov OG, Burueva DB, Barskiy DA, Bukhtiyarova GA, Kovtunov KV, Koptyug IV (2015) A mechanistic study of thiophene hydrodesulfurization by the parahydrogen-induced polarization technique. *Chemcatchem* 7:3508–3512
46. Sullivan DL, Ekerdt JG (1998) Mechanisms of thiophene hydrodesulfurization on model molybdenum catalysts. *J Catal* 178:226–233
47. Blake MR, Eyre M, Moyes RB, Wells PB (1981) Deuterium tracer study of some hydrodesulphurisations catalysed by powdered molybdenum disulphide. In: Seivama T, Tanabe K (eds) *Studies in surface science and catalysis*. Elsevier, Amsterdam, pp 591–603
48. McCarty KF, Schrader GL (1987) Deuterodesulfurization of thiophene: an investigation of the reaction mechanism. *J Catal* 103:261–269

**Publisher's Note** Springer Nature remains neutral with regard to jurisdictional claims in published maps and institutional affiliations.